Electronic Supplementary Material (ESI) for Physical Chemistry Chemical Physics.

Electronic Supplementary Information

In situ Reversible Redox Switching of First Hyperpolarizability of bimetallic Ruthenium complexes

Karthika C., Sarath Kumar S. R., Kathuria L., Das* P. K., and Samuelson A. G.,

Department of Inorganic and Physical Chemistry, Indian Institute of Science, Bangalore 560012, India

Figure S1. (a)1H NMR of $Ru(acac)_2(CH_3CN)_2$, **1** and (**b**) [$(acac)_2$Ru-bptz-$Ru(acac)_2$], **2** in $CDCl_3$

(a)

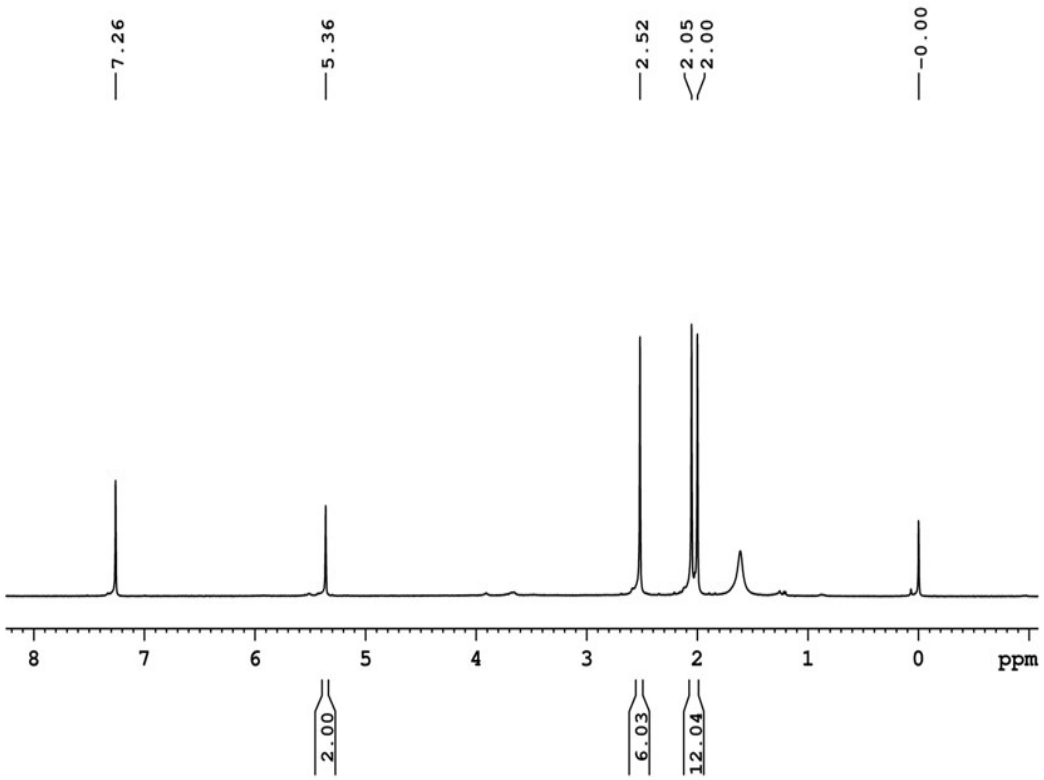

(**b**)

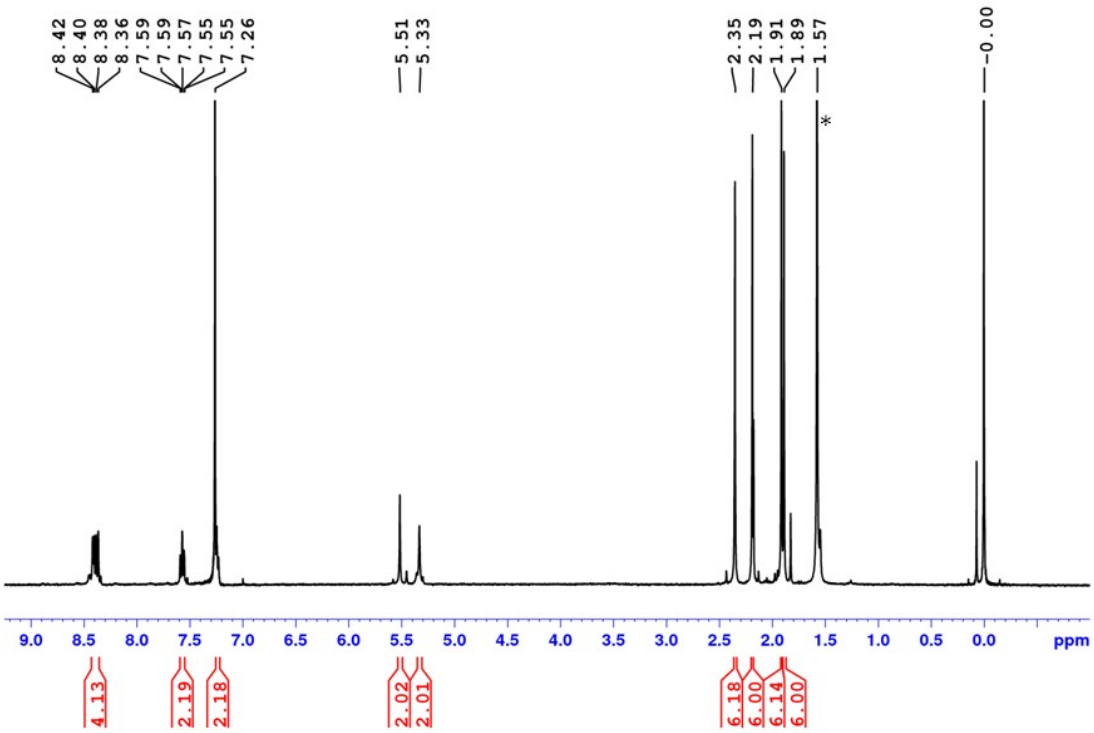

* Indicates a signal of water impurity.

Figure S2. ESI-MS data of the **(a)** monometallic, **1** and **(b)** bimetallic

(a)

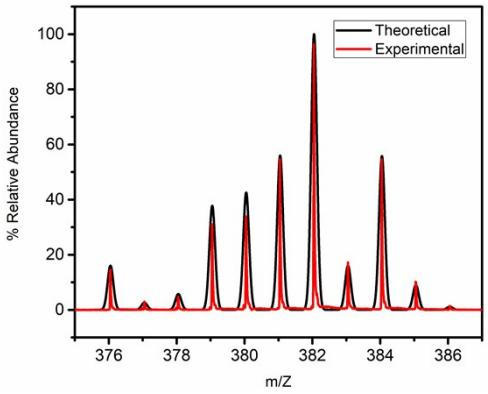

(b)

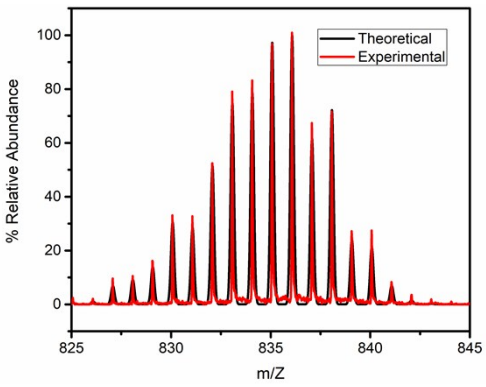

Figure S3. Quadratic dependence of $I_{2\omega}$ on I_{ω} for complex **2** in CH_2Cl_2 ($6x10^{-5}$ M). The experimental data were fitted with the straight line of the form $\ln I_{2\omega}=\ln A+n \ln I_{\omega}$. Where $I_{2\omega}$ is the output power, I_{ω} is the input power, A is proportionality constant and n is the order of process. Here the value of n extracted from the fit is 2.03.

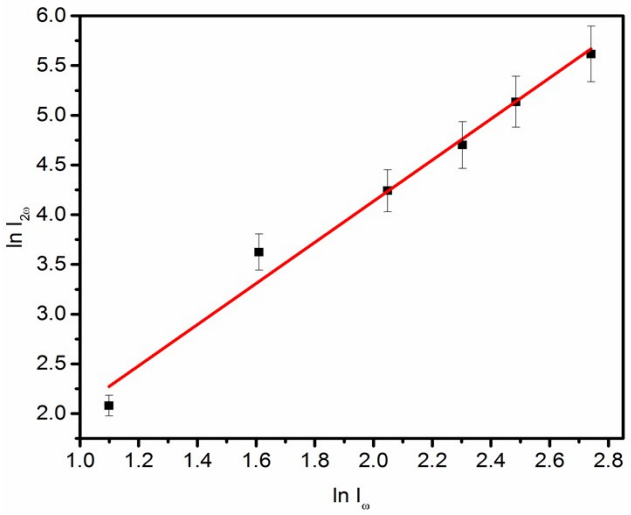

Figure S4. Wavelength scan of SHLS signal for complex **2** in CH_2Cl_2 ($1x10^{-5}$ M, 10 mJ/ pulse)

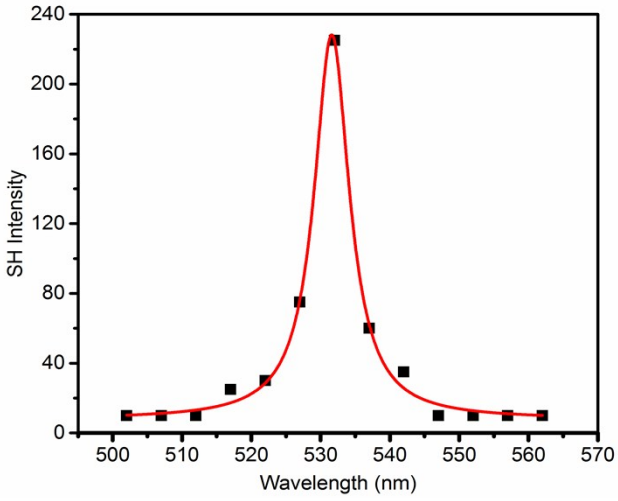

Figure S5: XYZ coordinates of optimized geometries **(a)** monometallic, **1** and **(b)** bimetallic, **2**

(a) **(b)**

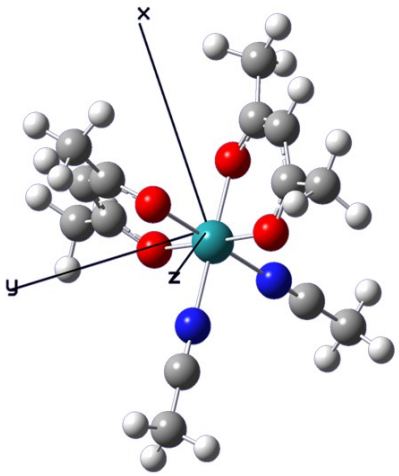

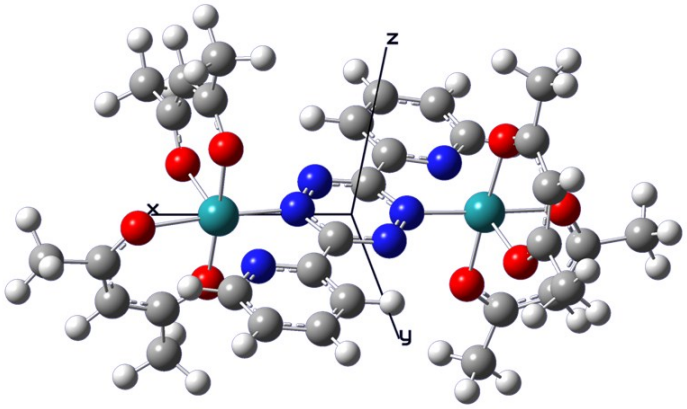

Mono, **1**

	X	Y	Z
C	2.04467	1.80979	-0.71525
C	2.80037	1.51587	0.43409
C	2.50953	0.56032	1.42689
C	2.53195	2.90145	-1.6458
C	3.4579	0.42595	2.60164
O	0.96049	1.25139	-1.07626
O	1.51308	-0.2272	1.45685
Ru	0.00005	-0.2542	-0.00152
O	-0.9689	1.2397	1.08152
C	-2.05549	1.79507	0.72318
C	-2.54866	2.87857	1.66015
C	-2.8092	1.50419	-0.42822
C	-2.51374	0.55498	-1.42571
C	-3.46124	0.42211	-2.60134
O	-1.51369	-0.22782	-1.45936
N	1.01582	-1.66857	-1.06658
N	-1.00605	-1.68052	1.05725
C	1.58601	-2.45391	-1.6883
C	-1.56944	-2.47094	1.67873
C	2.30136	-3.44409	-2.47445
C	-2.27546	-3.46633	2.46675

H	3.70098	2.09941	0.57826
H	3.48429	3.32978	-1.33299
H	2.63698	2.50248	-2.6585
H	1.78578	3.70008	-1.69336
H	4.31243	1.09929	2.53397
H	2.91982	0.63224	3.53138
H	3.82231	-0.60329	2.66495
H	-1.80351	3.67741	1.71841
H	-3.49987	3.30847	1.34608
H	-2.65869	2.471	2.66893
H	-3.71235	2.08443	-0.56972
H	-4.31861	1.09155	-2.53078
H	-2.9238	0.63495	-3.52998
H	-3.82137	-0.60833	-2.66953
H	2.94857	-2.95156	-3.20258
H	2.91745	-4.06945	-1.82556
H	1.59607	-4.0827	-3.00975
H	-1.62454	-4.31914	2.66884
H	-2.59359	-3.03646	3.41848
H	-3.15797	-3.81871	1.9295

Bimetallic, **2**

Ru	-3.35231	-0.06027	0.02414
Ru	3.35245	0.06017	0.02401
O	-5.42069	-0.3669	-0.18325
O	-3.18791	0.09827	-2.05444
O	-3.62665	-0.19586	2.08311
O	-3.77445	1.99473	0.06792
O	5.42074	0.36688	-0.18363
O	3.18777	-0.09896	-2.05445
O	3.62684	0.19633	2.083
O	3.77452	-1.99485	0.06838
N	-2.82662	-2.07367	-0.00035
N	-1.3617	0.08117	0.15476
N	-0.64572	1.20516	0.14208
N	0.64582	-1.20533	0.14218
N	1.36178	-0.08135	0.15479
N	2.82669	2.07354	-0.00076
C	-0.6669	-1.1049	0.13124
C	-1.49371	-2.31457	0.07893
C	-0.97149	-3.60461	0.10879
H	0.10009	-3.74108	0.1691
C	-1.84815	-4.68147	0.06154

H	-1.47072	-5.69689	0.08355
C	-3.21755	-4.43197	-0.00965
H	-3.93564	-5.24216	-0.04281
C	-3.66822	-3.11828	-0.03728
H	-4.72084	-2.87166	-0.08472
C	0.66699	1.10471	0.13118
C	1.49379	2.3144	0.07879
C	0.97152	3.60441	0.10891
H	-0.10005	3.74081	0.16948
C	1.84811	4.68132	0.0616
H	1.47065	5.69672	0.08384
C	3.21751	4.43187	-0.00992
H	3.93556	5.24209	-0.04316
C	3.66822	3.11821	-0.03778
H	4.72085	2.87166	-0.08545
C	-6.07017	-0.2899	-1.27533
C	-5.52424	-0.06997	-2.55194
H	-6.22185	-0.03656	-3.37885
C	-4.16503	0.09935	-2.8702
C	-7.56703	-0.46832	-1.14077
H	-7.78309	-1.4398	-0.68696
H	-8.08848	-0.40168	-2.09557
H	-7.96569	0.2943	-0.46579
C	-3.77444	0.30771	-4.31743
H	-3.04682	-0.45239	-4.61474

H	-3.28442	1.2795	-4.42603
H	-4.62737	0.26594	-4.99461
C	-3.95571	0.7882	2.82709
C	-4.16731	2.11574	2.42479
H	-4.4409	2.81493	3.20454
C	-4.07571	2.63872	1.11832
C	-4.1271	0.43204	4.28805
H	-4.89686	-0.33846	4.38784
H	-4.40445	1.28896	4.90162
H	-3.19663	0.0061	4.67394
C	-4.35568	4.11166	0.90497
H	-3.46459	4.59791	0.49747
H	-4.64806	4.62437	1.82129
H	-5.15063	4.22881	0.16352
C	6.07007	0.29007	-1.27579
C	5.52396	0.07014	-2.55235
H	6.22145	0.03698	-3.37937
C	4.16479	-0.09969	-2.87039
C	7.56694	0.46856	-1.14144
H	7.96599	-0.2953	-0.46809
H	7.783	1.43918	-0.68584
H	8.08806	0.40377	-2.09656
C	3.77401	-0.30818	-4.31754
H	3.2841	-1.28004	-4.42604
H	4.62683	-0.26632	-4.99485

H	3.04624	0.45182	-4.61477
C	3.95589	-0.78753	2.82723
C	4.1673	-2.11522	2.4253
H	4.44079	-2.81422	3.20526
C	4.07557	-2.63859	1.11901
C	4.12774	-0.43093	4.28804
H	3.19843	-0.00189	4.67328
H	4.89984	0.33729	4.38762
H	4.40236	-1.28826	4.90226
C	4.35493	-4.11171	0.90618
H	3.463	-4.59809	0.50067
H	4.6488	-4.62384	1.82236
H	5.1485	-4.22955	0.16338

Figure S6. Molecular orbitals involved in transitions of Ruthenium complexes obtained from TD-DFT calculations.

Complex	λ^{theory} (nm)	oscillator strength	Transitions (% contributions)
1	310	0.0281	HOMO → LUMO (89)
$\mathbf{1}^{+}$	321	0.0038	HOMO-3(α) →LUMO+2 (α) (48) HOMO(α) → LUMO(α) (34) HOMO-2(α) →LUMO+3(α) (17)
	528	0.65	HOMO(β) → LUMO(β) (91)
2		0.438	HOMO→ LUMO+1 (44) HOMO→ LUMO (22) HOMO-2 →LUMO(20)
$\mathbf{2}^{+}$	632	0.362	HOMO-1(β) →LUMO(β) (52) HOMO-1(α) → LUMO(α) (42)
	1400	0.0154	HOMO LUMO(72)
$\mathbf{2}^{2+}$	501	0.217	HOMO-3 (β) →LUMO+3 (β) (39) HOMO-2(β) →LUMO+1(β) (24.5) HOMO-2 (β) →LUMO+4(β) (15)

Figure S7. Molecular orbitals involved in major contributing transitions of Ruthenium complexes obtained from TD-DFT calculations.

Complex	λ^{theory} (nm)	Ground State	Excited State
1	310 (π-π^*)	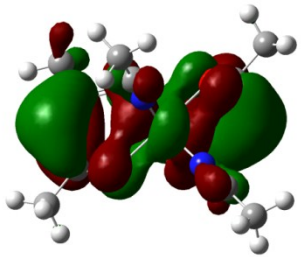	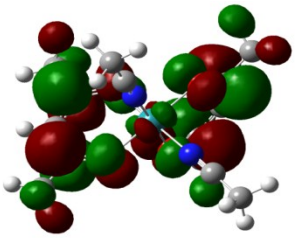
1$^+$	319 (π-π^*)	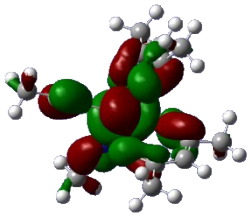	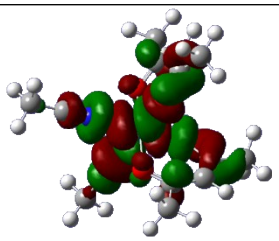
	600 (LMCT)	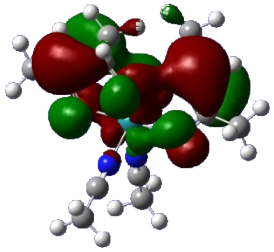	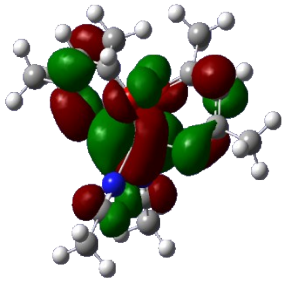
2	555 (MLCT)	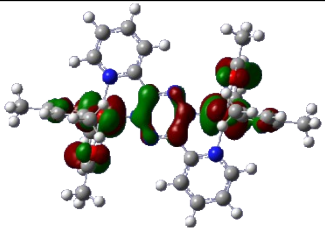	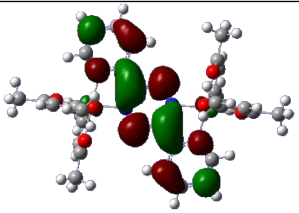

2^{+}	632 (MLCT)	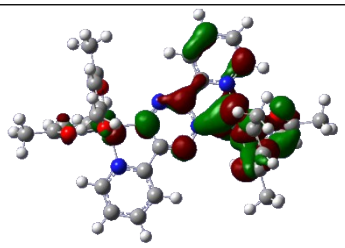	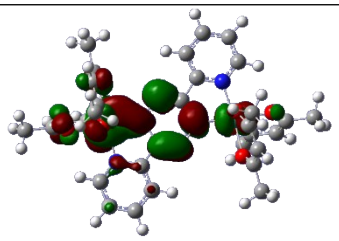
	1400 (IVCT)	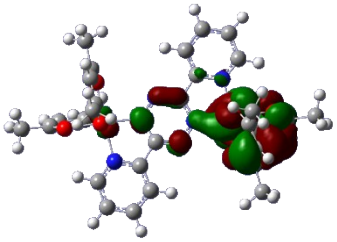	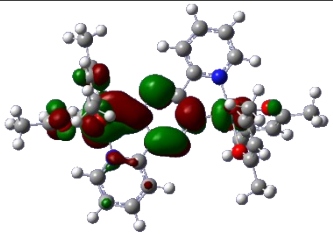
2^{2+}	501 (LMCT)	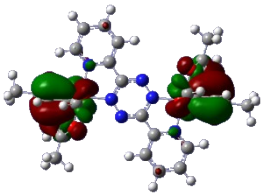	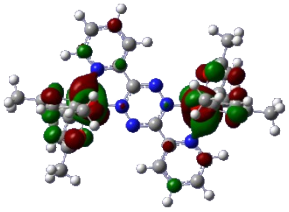

Figure S8.TD- DFT predicted frontier orbitals of complexes and their percentage composition

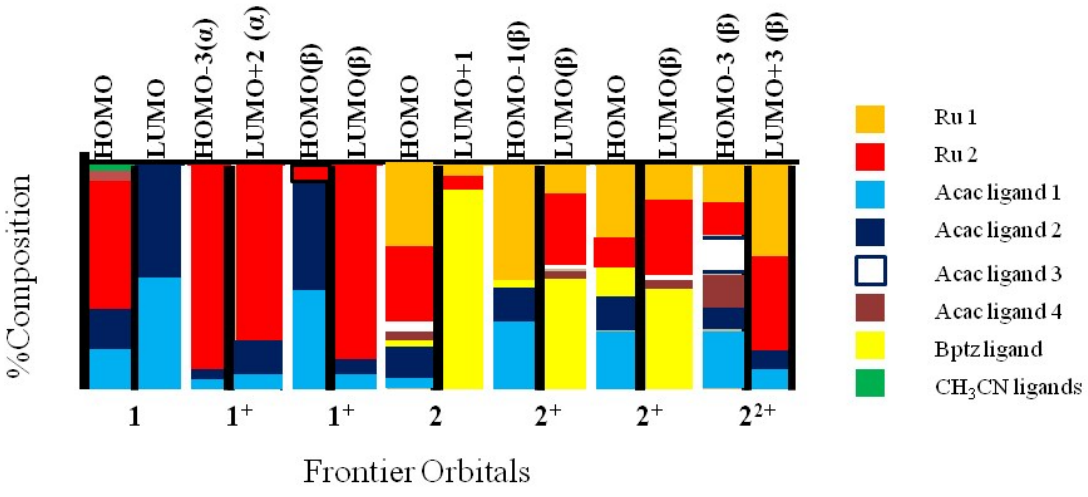

Figure S9. Peak current dependence on concentration of mononuclear Ru complex at 40 mV/s

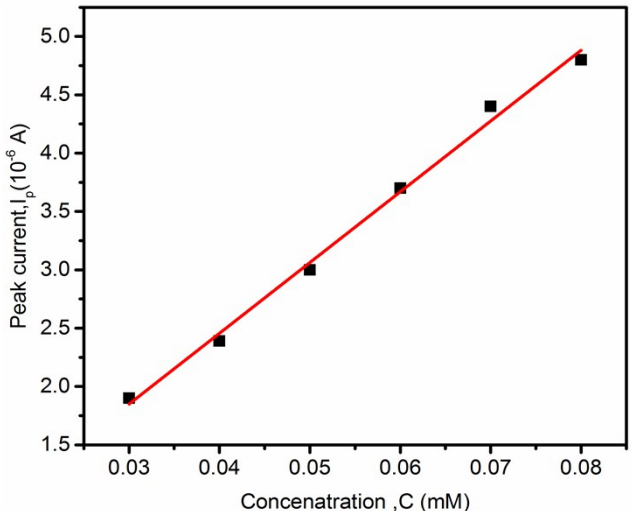

Figure S10. Peak current dependence on square root of scan rate, υ of mononuclear Ru complex

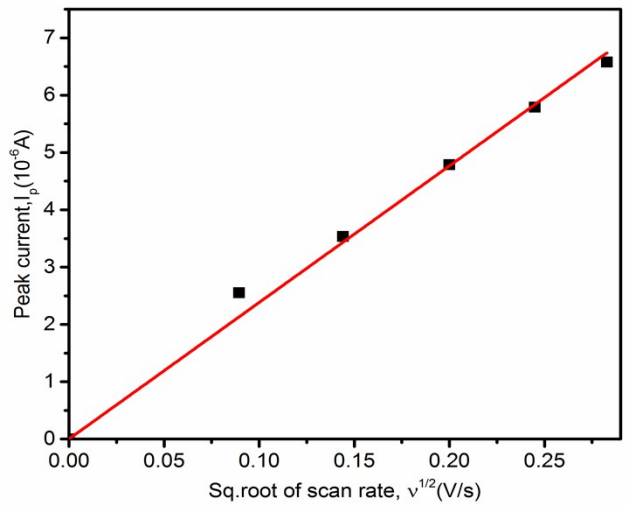

.

Figure S11. Bulk electrolysis of complex, **1** (10^{-5} M) at 0.35 V for 30 minutes

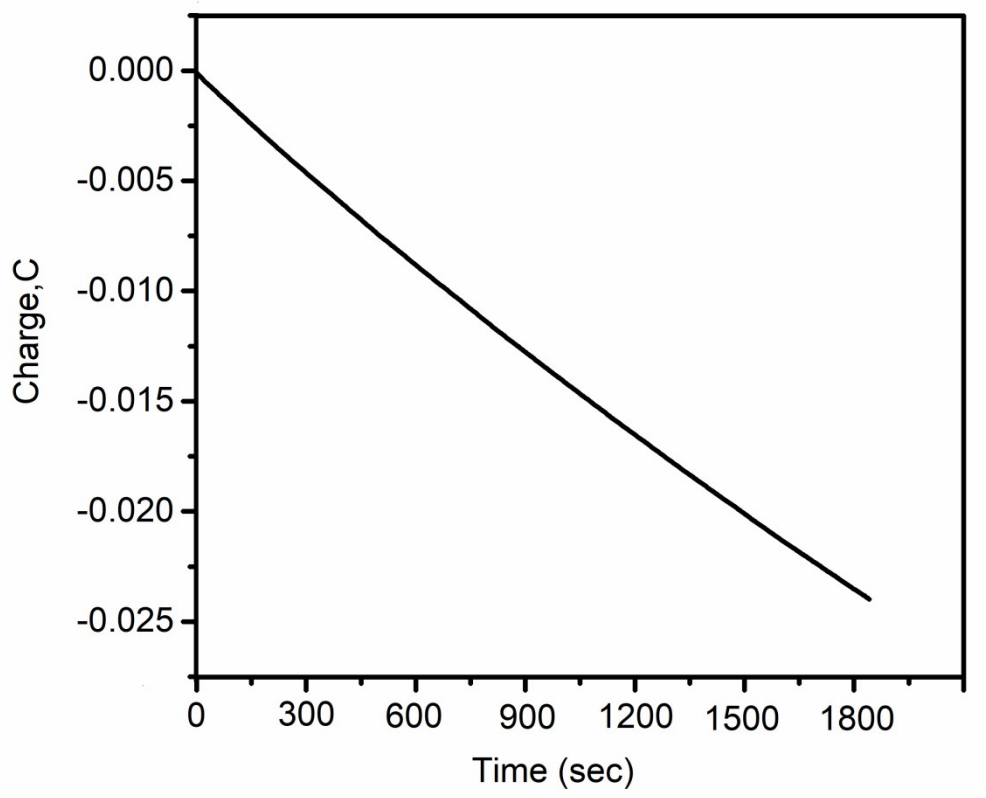

Figure S12. Concentration dependence studies of (a) Complex $\mathbf{1}^{+}$ (b) Complex $\mathbf{2}^{+}$ (c) Complex $\mathbf{2}^{2+}$

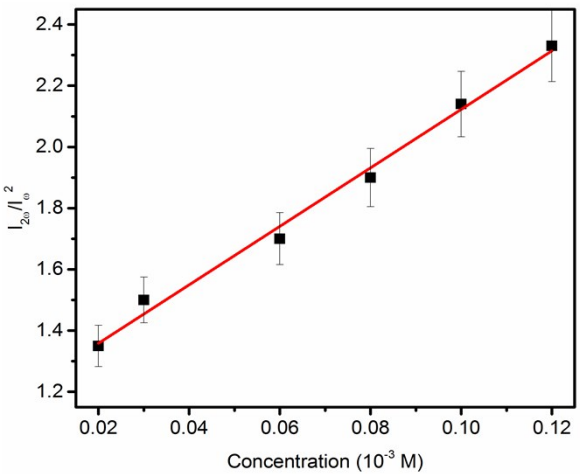

(a) Complex $\mathbf{1}^{+}$

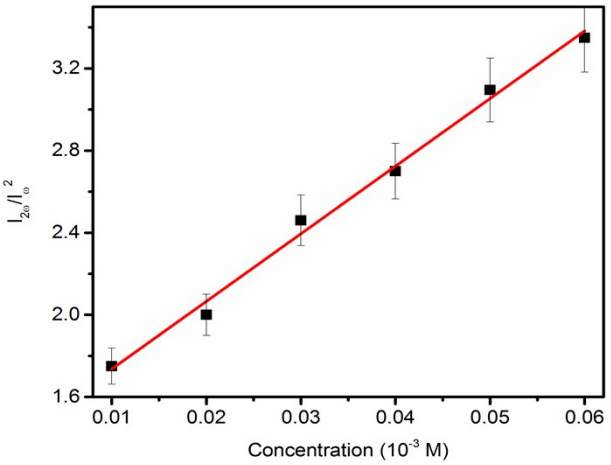

(b) Complex $\mathbf{2}^{+}$

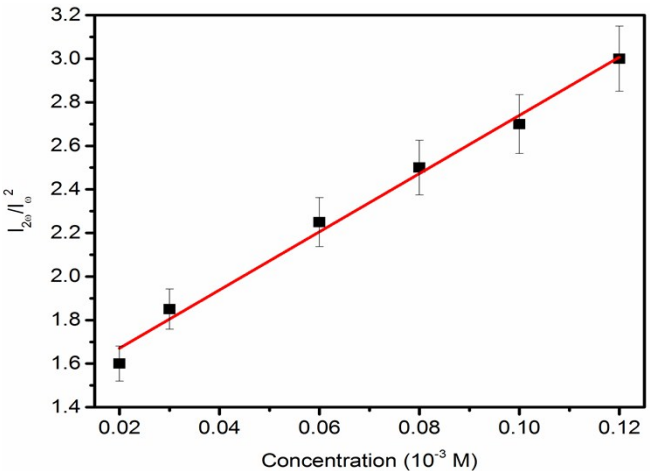

(c) Complex $\mathbf{2}^{2+}$